

Bioactive cyclometalated phthalimides: design, synthesis and kinase inhibition†Sebastian Blanck,^a Yann Geisselbrecht,^a Katja Kräling,^a Stephen Middel,^a Thomas Mietke,^a Klaus Harms,^a Lars-Oliver Essen^a and Eric Meggers^{*a,b}

Received 30th April 2012, Accepted 7th June 2012

DOI: 10.1039/c2dt30940h

The regioselective cyclometalation of 4-(pyridin-2-yl)phthalimide was exploited for the economical design of organometallic protein kinase inhibitors. 4-(Pyridin-2-yl)phthalimide can be prepared from inexpensive 4-bromophthalimide in just three steps including one Pd-catalyzed Stille cross-coupling. The versatility of this new ligand was demonstrated with the synthesis of ruthenium(II) half-sandwich as well as octahedral ruthenium(II) and iridium(III) complexes. The regioselectivity of the C–H activation in the course of the cyclometalation can be influenced by the reaction conditions and the steric demand of the introduced metal complex fragment. The biological activity of this new class of metalated phthalimides was evaluated by profiling two representative members against a large panel of human protein kinases. A cocrystal structure of one metallo-phthalimide with the protein kinase Pim1 confirmed an ATP-competitive binding with the intended hydrogen bonding between the phthalimide moiety and the hinge region of the ATP-binding site.

Introduction

Metal complexes are highly versatile structural scaffolds for the molecular recognition of biomolecules such as nucleic acids and proteins.^{1–4} Over the last several years our laboratory contributed to this area of research with the design of substitutionally inert ruthenium(II),⁵ osmium(II),⁶ rhodium(III),⁷ iridium(III),⁸ and platinum(II)⁹ complexes as highly potent and selective ATP-competitive inhibitors of protein kinases and lipid kinases.¹⁰ Our previous design was mainly inspired by the natural product staurosporine with the maleimide moiety of pyridocarbazole metal complexes (Fig. 1) undergoing hydrogen bonding with the hinge region of the ATP-binding site, with the pyridocarbazole heterocycle occupying the hydrophobic adenine binding cleft, and the remaining coordination sphere interacting with the region of the ribose-triphosphate binding site and thereby strongly contributing to binding affinity and selectivity.¹¹ However, the synthesis of the pyridocarbazole heterocycle is cumbersome and contains a photochemical step which is difficult to scale.¹² Furthermore, due to an intrinsic binding bias of the pyridocarbazole moiety we estimate that only a subset of the more than 500 human protein kinases are suitable targets for the metallo-pyridocarbazole scaffold.¹³ To address these limitations we recently

introduced a new class of cyclometalated metal complexes with the ligand 3-(pyridin-2-yl)-1,8-naphthalimide and we demonstrated their suitability for the development of nanomolar protein kinase inhibitors.^{14,15} It turned out that a drawback of this scaffold is manifested by the steric interference between the ligand sphere of the metal complexes and the 5-position of the naphthalene moiety (highlighted in Fig. 1), resulting in a distortion of the octahedral coordination geometry and thus rendering structure-based inhibitor design somewhat more complicated. Our recent studies have hence focused on a smaller, sterically less demanding ligand for cyclometalation and we developed 4-(pyridin-2-yl)phthalimide as a novel ligand for the highly efficient design of cyclometalated metallo-phthalimide protein kinase inhibitors. In a preliminary report we found a ruthenium phthalimide complex as a nanomolar inhibitor of the p21 activated kinase 1 (PAK1) and confirmed its ATP-competitive binding by an X-ray cocrystal structure.¹⁶ We here provide a full account on the design, synthesis, and kinase inhibition of cyclometalated pyridylphthalimide complexes and present a new cocrystal structure of a metallo-pyridylphthalimide bound to the ATP-binding site of the protein kinase Pim1.

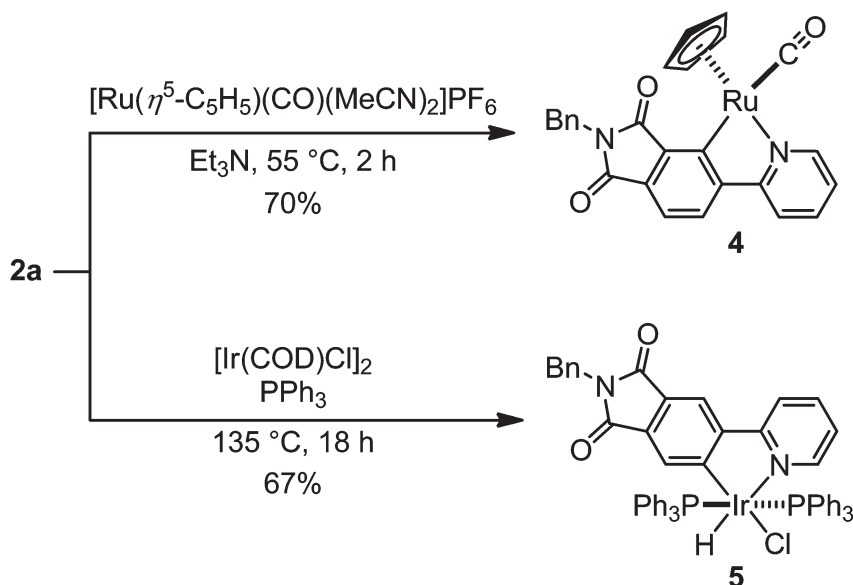
Results and discussion**Pyridylphthalimide ligand synthesis**

N-Benzyl-4-bromophthalimide (**1a**) and *N*-(*tert*-butyldimethylsilyl)-4-bromophthalimide (**1b**) were converted to *N*-benzyl-4-(pyridin-2-yl)phthalimide (**2a**) and *N*-(*tert*-butyldimethylsilyl)-4-(pyridin-2-yl)phthalimide (**2b**) using palladium-mediated Stille cross-coupling with 2-(trimethylstannyl)pyridine and

^aFachbereich Chemie, Philipps-Universität Marburg, Hans-Meerwein-Straße, 35043 Marburg, Germany

^bDepartment of Chemical Biology, College of Chemistry and Chemical Engineering, Xiamen University, Xiamen 361005, P.R. China.
E-mail: meggers@chemie.uni-marburg.de

†Electronic supplementary information (ESI) available. CCDC 861334–861338. For ESI and crystallographic data in CIF or other electronic format see DOI: 10.1039/c2dt30940h



Scheme 2 Regioselective C–H activation of ligand **2a**. Synthesis of the pseudo-octahedral ruthenium half-sandwich complex **4** and the octahedral iridium complex **5**.

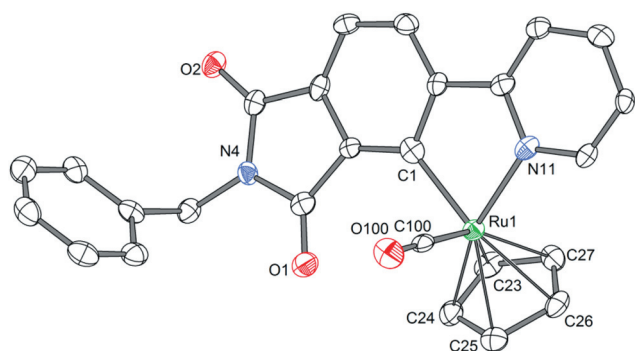


Fig. 2 Crystal structure of ruthenium half-sandwich complex **4**. ORTEP drawing with 50% probability thermal ellipsoids. Selected bond distances (Å): C1–Ru1 = 2.048(4), N11–Ru1 = 2.089(3), C100–Ru1 = 1.827(4), C23–Ru1 = 2.264(4).

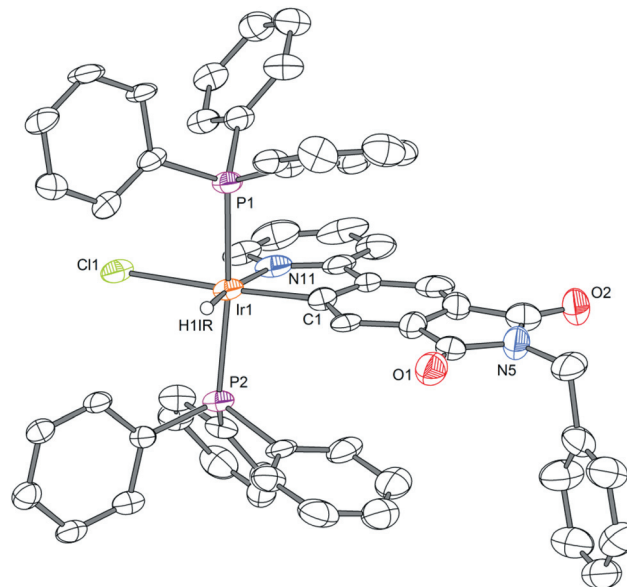


Fig. 3 Crystal structure of iridium(III) complex **5**. ORTEP drawing with 50% probability thermal ellipsoids. Selected bond distances (Å): C1–Ir1 = 2.001(8), N11–Ir1 = 2.126(7), Cl1–Ir1 = 2.483(2), P1–Ir1 = 2.3417(18), P2–Ir1 = 2.3300(17).

hydride are arranged within the plane of the pyridylphthalimide moiety *cis* and *trans* to the pyridine ligand, respectively, whereas the two bulky triphenylphosphines are coordinated at the axial positions. Despite the coordinated hydrido ligand, which is strongly shifted up-field in the $^1\text{H-NMR}$ to -16.58 ppm, as well as the carbon–iridium bond, the complex is very robust and can be easily handled under air. This is most likely due to the two bulky triphenylphosphine ligands shielding the metal center from further reactions.

It can be assumed that in these two reactions the regioselectivity of the C–H activation is strongly influenced by steric effects, with small metal fragments preferring a cyclometalation with C-3, probably directed by a transient coordination to the neighboring maleimide carbonyl group, whereas more bulky metal fragments prefer the sterically less congested cyclometalation with C-5.

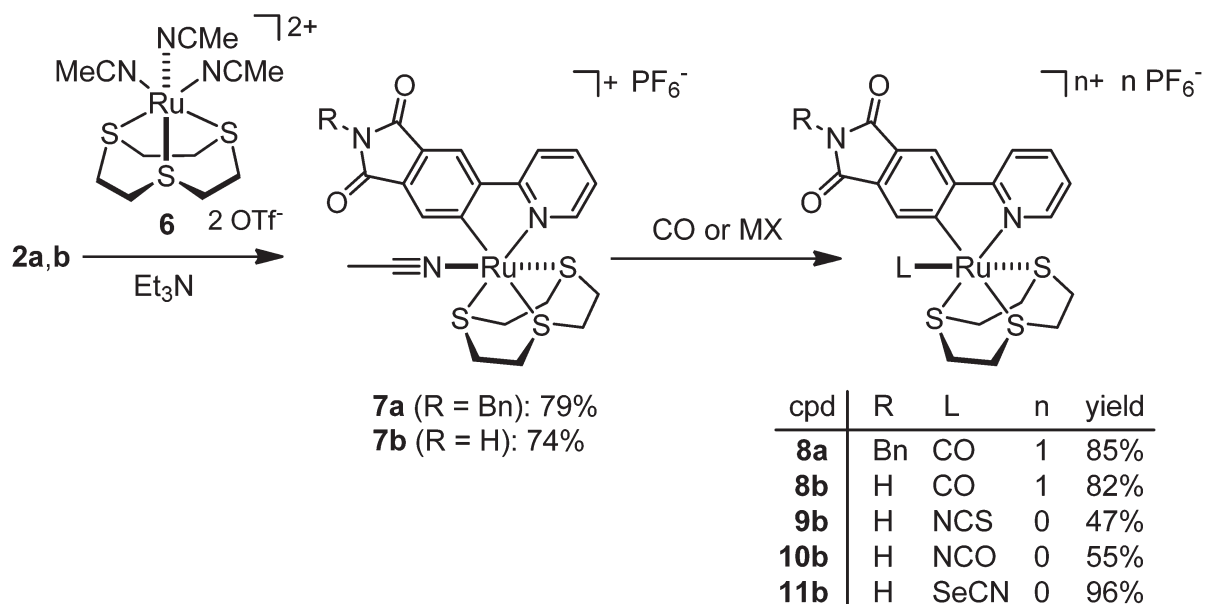
Synthesis of bioactive metal complexes

Guided by simple molecular modeling experiments we concluded that the cyclometalation at the 5-position of the phthalimide moiety should be preferred for the generation of protein kinase inhibitors. We therefore decided to synthesize ruthenium pyridylphthalimide complexes containing the facial tridentate ligand 1,4,7-trithiacyclononane since it not only prevents the formation of diastereomers due to its high symmetry but we also expected that due to its bulkiness it would guide the

cyclometalation to the C-5 position. Indeed, the reaction of the pyridylphthalimide ligands **2a** or **2b** with $[\text{Ru}(\text{MeCN})_3][9\text{-aneS}_3](\text{CF}_3\text{SO}_3)_2$ (**6**)¹⁸ ($9\text{-aneS}_3 = 1,4,7\text{-trithiacyclononane}$) afforded the monoacetonitrile complexes **7a** (79%) or **7b** (74%), respectively, with high regioselectivity (Scheme 3).

A crystal structure of complex **7b** is shown in Fig. 4 and confirms the coordination of ruthenium to the pyridine ligand including a cyclometalation at the 5-position of the phthalimide. The structure also nicely reveals the ability of the maleimide moiety to form a donor and acceptor hydrogen bond with the

imide NH and carbonyl CO, respectively. The semilabile acetonitrile ligand is prone to substitution against other anionic or neutral monodentate ligands as has been demonstrated in related systems.¹⁹ For example, the reaction of **7a** or **7b** with CO in DMF at 95 °C for 3 h afforded the CO-complexes **8a** (85%) or **8b** (82%), respectively, whereas the reaction of **7b** with NaSCN, NaOCN, and KSeCN afforded the complexes **9b** (N-bound isomer, 47%), **10b** (N-bound isomer, 55%), and **11b** (Se-bound isomer, 96%), respectively. A crystal structure of complex **8a** is displayed in Fig. 5 and demonstrates the expected almost



Scheme 3 Synthesis of a library of bioactive octahedral metal complexes **8a,b** and **9b–11b** via regioselective C–H-activation at the 5-position of the phthalimide moiety followed by a ligand substitution reaction. MX = NaOCN, NaSCN, or KSeCN.

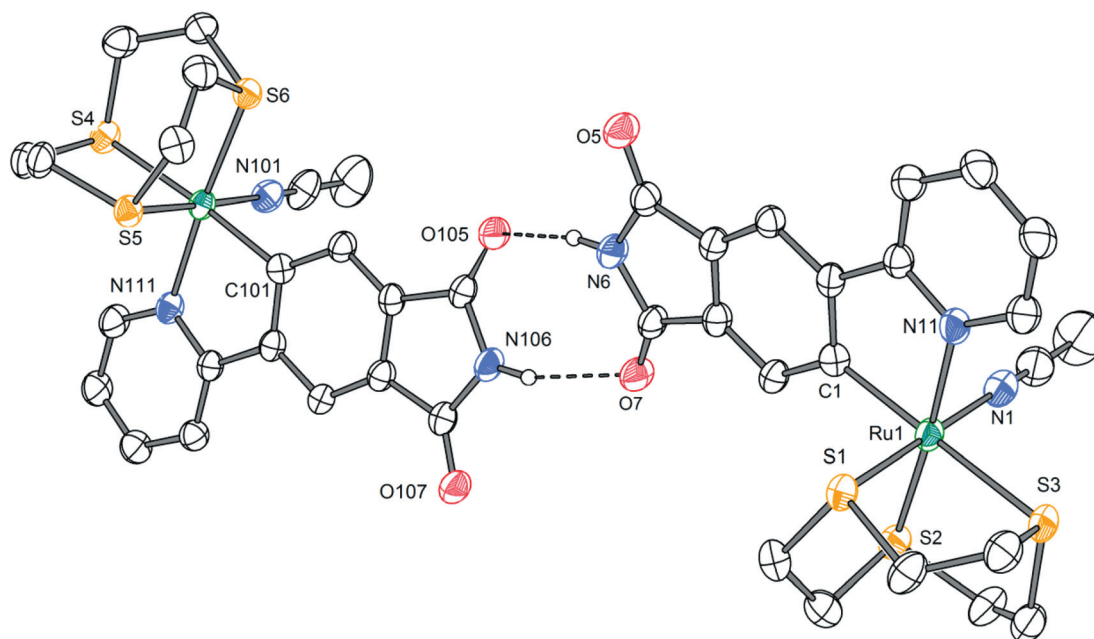


Fig. 4 Crystal structure of ruthenium acetonitrile complex **7b**. A solvent molecule of diethyl ether and a hexafluorophosphate counter ion are omitted for clarity. ORTEP drawing with 50% probability thermal ellipsoids. Selected bond distances (Å): C1–Ru1 = 2.039(4), N11–Ru1 = 2.093(3), N1–Ru1 = 2.055(4), S1–Ru1 = 2.2988(10), S2–Ru1 = 2.2988(10), S3–Ru1 = 2.4108(9).

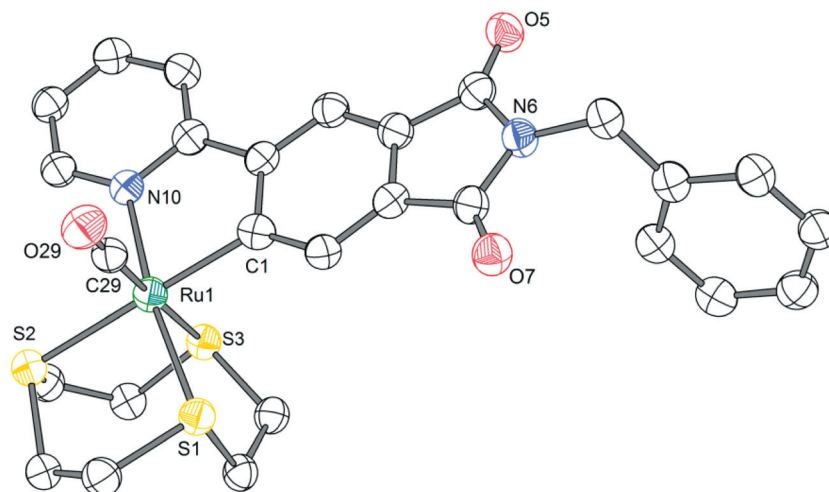


Fig. 5 Crystal structure of the *N*-benzylated complex **8a**. The hexafluorophosphate counter ion is omitted for clarity. ORTEP drawing with 50% probability thermal ellipsoids. Selected bond distances (Å): C1–Ru1 = 2.055(4), N10–Ru1 = 2.105(3), C29–Ru1 = 1.859(4), S1–Ru1 = 2.3297(11), S2–Ru1 = 2.4235(10), S3–Ru1 = 2.4102(11).

perfectly octahedral coordination around the ruthenium, as compared to a strongly distorted octahedral coordination sphere around the ruthenium center in the related pyridylphthalimide complex (Fig. 1).¹⁴

Protein kinase profiling

To gain insight into the protein kinase inhibition properties of pyridylphthalimide metal complexes, complexes **8b** and **9b** were profiled against the majority of the human protein kinases encoded in the human genome (human kinome).¹³ This was accomplished by using an active-site-directed competition binding assay with 442 different protein kinases (KINOMEscan, DiscoverX) which provides primary data (%ctrl = percent of control: 0% = highest affinity; 100% = no affinity) that correlate with binding constants (K_d).^{20,21} Interestingly, although these two complexes should be capable of forming hydrogen bonds between the maleimide moiety and all profiled protein kinases, the screening data demonstrated surprisingly high selectivities, with the CO-complex **8b** only binding strongly to 15 and the NCS-complex **9b** only to 5 protein kinases with %ctrl < 1% (Fig. 6). The observed high selectivity is consistent with all our previous studies on the kinase inhibition properties using octahedral metal complexes and we hypothesize that this is due to the space-demanding, defined globular shapes of the octahedral inhibitors that are very sensitive even to small differences in the structure and dynamics of the kinase ATP-binding sites. Interestingly, the somewhat lower kinase selectivity of complex **9b** as compared to **8b** might be due to the rotational freedom of the coordinated NCS ligand which is absent in the CO-complex **8b**. It is also interesting to note that although **8b** and **9b** only differ by a single monodentate ligand, both complexes target completely different subsets of protein kinases as visualized by the kinase dendrograms shown in Fig. 6.

Protein kinase binding

Whereas the binding of the NCS-complex **9b** to the protein kinase PAK1 was reported by us recently,¹⁶ we were interested in

understanding the protein kinase binding mode of the more selective CO-complex **8b** and we therefore cocrystallized the racemate of **8b** with Pim1. The structure of the Pim1–**8b** complex was determined and refined to a resolution of 2.3 Å. The overall structure is shown in Fig. 7 and reveals the typical two-lobe protein kinase architecture with the catalytic ATP-binding site positioned in a deep intervening cleft and occupied by the ruthenium complex **8b**. The maleimide moiety of **8b** forms one hydrogen bond between the NH and the backbone carbonyl group of Glu121, whereas a second hydrogen bond is prevented by Pro123 (Fig. 8). A significant number of hydrophobic contacts are formed with the pyridylphthalimide, the 1,4,7-trithiacyclononane, and the CO ligand. The ruthenium-coordinated CO ligand points towards the flexible glycine-rich loop (P-loop) and fills a small hydrophobic pocket that is formed by induced fit. The same unusual interaction between coordinated CO and the glycine-rich loop has been frequently observed with the previously established metallo-pyridocarbazole kinase inhibitors.^{5,6,22} Interestingly, a comparison of this Pim1–**8b** structure with the cocrystal structure of complex **9b** and PAK1 (PDB ID: 4DAW)¹⁶ reveals some significant differences. Firstly, the binding orientation of the pyridylphthalimide within the ATP-binding sites differs with a preference for opposite metal-centered stereoisomers (Fig. 9). Secondly, whereas the NCS ligand of **9b** points towards the interface of the glycine-rich loop and the adjacent β -sheet, the CO of **8b** is located right below the glycine-rich loop. Thus, although **8b** and **9b** differ only by the nature of a single monodentate ligand, their binding modes within the ATP-binding sites diverge, thus explaining the distinguished kinase profiling results of **8b** and **9b**.

Conclusions

In summary, we demonstrated the merit of 4-(pyridin-2-yl)-phthalimide for the straightforward generation of metal-based protein kinase inhibitors. The imide moiety is designed to hydrogen bond with the hinge region of the ATP-binding site, whereas the metal coordination to the pyridine with concomitant

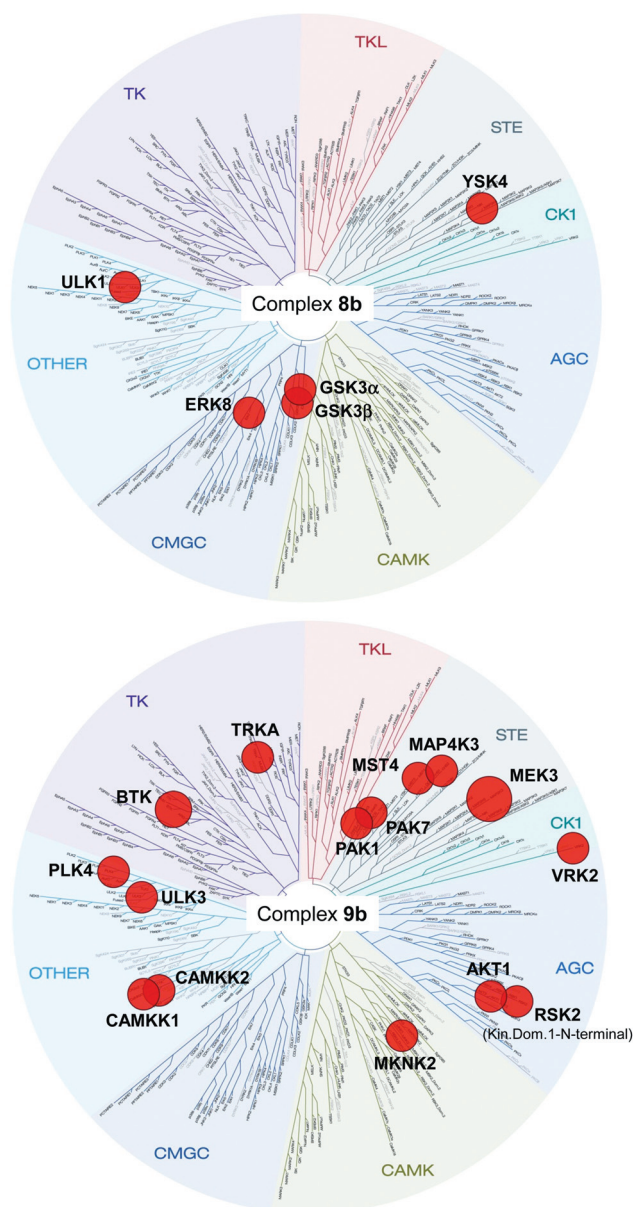


Fig. 6 Binding selectivities of complexes **8b** and **9b** within the human protein kinase dendrogram which displays the protein kinase families and the evolutionary relationships between the individual kinases (wild type). Determined by an active-site-directed affinity screening (KINOMEscan, DiscoveRx) against 442 human protein kinases. Shown are hits with %ctrl < 1% (below 1% of control; 0% = highest affinity, 100% = no affinity) at compound concentrations of 10 μ M. See ESI† for additional data.

regioselective cyclometalation to either C-3 or C-5 of the phthalimide moiety reduces the required number of coordinating heteroatoms. Thus, based on this simple pyridylphthalimide scaffold, selective protein kinase inhibitors can be synthesized in just a few steps in an economical fashion compared to the often tedious synthesis of our previously established staurosporine-inspired metallo-pyridocarbazoles. It is worth noting that the facile C–H activation and robustness of the formed metal–carbon bond can be attributed to the highly electron-deficient nature of

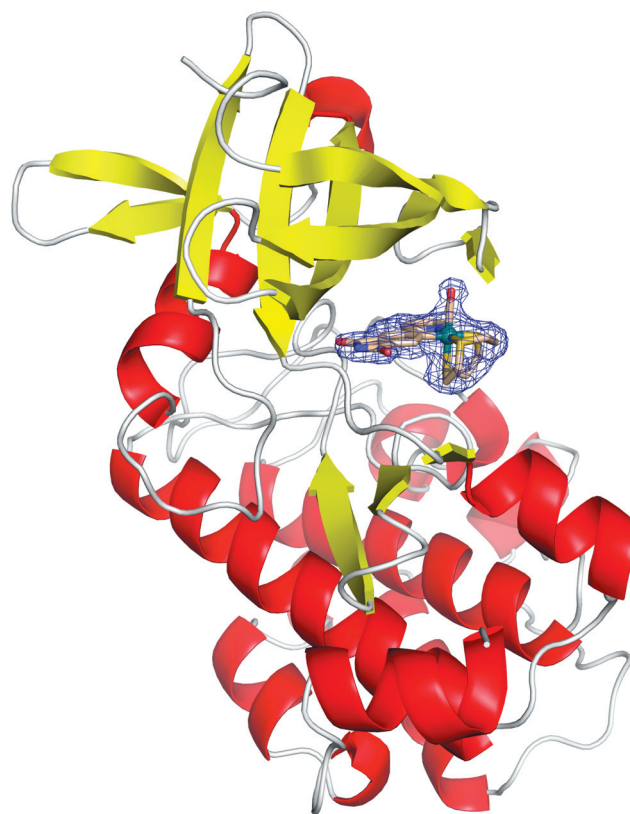


Fig. 7 Cocrystal structure of protein kinase Pim1 with one enantiomer of phthalimide **8b** bound to the ATP-binding site. The SIGMAA-weighted $2F_{\text{obs}} - F_{\text{calc}}$ difference electron density map of the ruthenium inhibitor was contoured at 1σ . Coordinates of the structure have been deposited in the Protein Data Bank (PDB ID: 4AS0).

the phthalimide moiety, being functionalized with electron-withdrawing pyridyl and maleimide substituents. Finally, we demonstrated the promising protein binding profiles of two pyridylphthalimide metal complexes and investigated the binding of one phthalimide complex to the ATP-binding site of the protein kinase Pim1. The investigation of the *in vitro* and *in vivo* properties of this novel class of bioactive metallo-phthalimides is underway.

Experimental section

General methods

All reactions were carried out using oven-dried glassware and conducted under a positive pressure of nitrogen unless specified otherwise. Chemicals were used as received from standard suppliers. 2-(Trimethylstannyl)pyridine,²³ tetrakis(triphenylphosphine)palladium(0),²⁴ [Ir(COD)Cl]₂,²⁵ [Ru(η^5 -C₅H₅)(CO)(MeCN)₂]₂PF₆,¹⁷ and [Ru(MeCN)₃([9]aneS₃)](CF₃SO₃)₂ (**6**)¹⁸ were prepared according to literature procedures. Phthalimides **1a**, **1b** were synthesized according to modified literature procedures (see ESI† for further details). All solvents for chromatography were distilled prior to use. Acetonitrile and DMF were dried by common methods and freshly distilled prior to use. NMR spectra were recorded on an Avance 300 (300 MHz), DRX

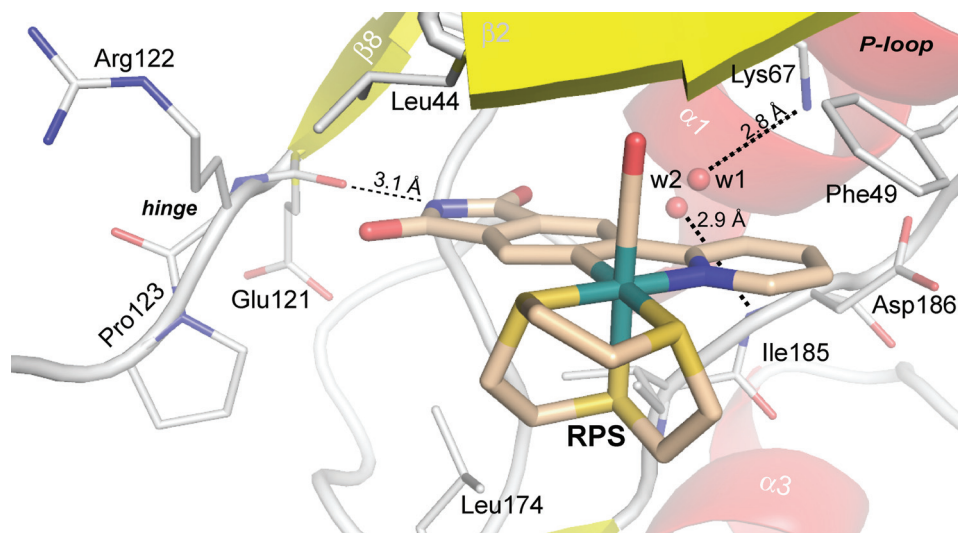


Fig. 8 Interactions of phthalimide **8b** (PDB ID: 4AS0, PDB ligand identifier **RPS**) within the active site of Pim1.

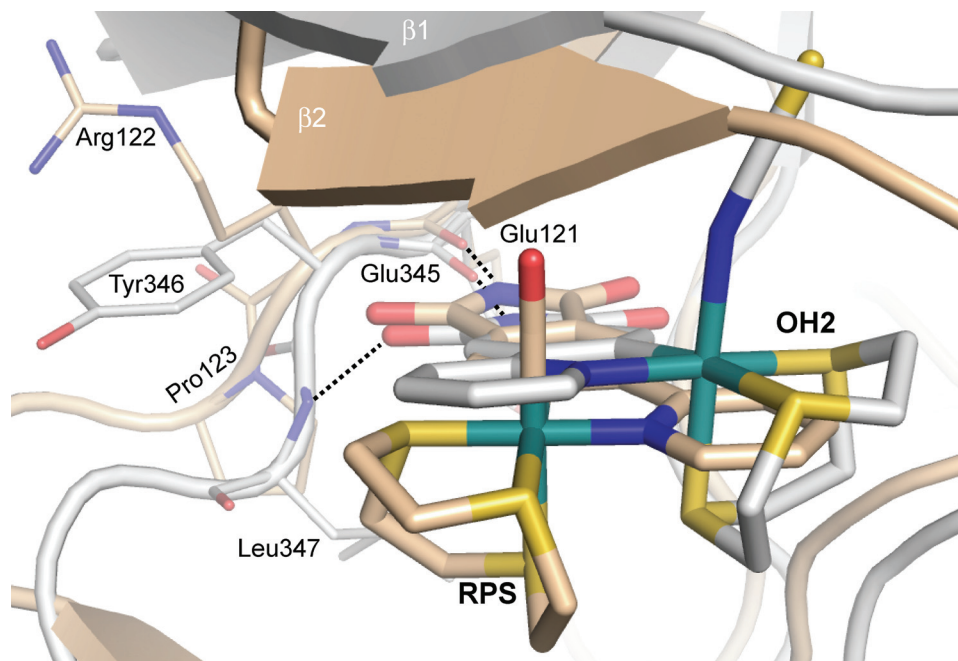


Fig. 9 Relative binding modes of **8b** (light brown, PDB ID: 4AS0, PDB ligand identifier **RPS**) and **9b** (white, PDB ID: 4DAW, PDB ligand identifier **OH2**) within the ATP-binding sites of Pim1 and PAK1, respectively. Superimposed with the PyMOL Molecular Graphics System, Version 1.3, Schrödinger, LLC.

500 (500 MHz), Avance 500 (500 MHz), or DPX-250 (250 MHz) spectrometer. Infrared spectra were recorded on a Bruker Alpha FTIR. High resolution mass spectra were obtained with a Finnigan LTQ-FT instrument using either APCI or ESI.

***N*-(Benzyl)-4-(pyridin-2-yl)phthalimide (2a).** *N*-Benzyl-4-bromophthalimide (**1a**) (1.28 g, 4.04 mmol) and 2-(trimethylstannyl)pyridine (0.90 g, 3.69 mmol) were dissolved in *m*-xylene (35 mL) and the solution was purged with nitrogen for 20 min. Tetrakis(triphenylphosphine)palladium(0) (473 mg, 0.41 mmol) was added and the solution heated to reflux under nitrogen for

48 h. The solution was cooled to ambient temperature, water (50 mL) was added, the organic phase was separated, and the aqueous phase was extracted with CH_2Cl_2 twice. The combined organic layers were washed with brine, dried using Na_2SO_4 , filtered, and the solvent removed *in vacuo*. The crude product was subjected to silica gel chromatography with first CH_2Cl_2 and then CH_2Cl_2 -MeOH 75 : 1. The combined product eluents were dried *in vacuo* and *N*-benzyl-4-(pyridin-2-yl)phthalimide (**2a**) was obtained as a light yellow solid (980 mg, 85%). $^1\text{H-NMR}$ (300 MHz, CDCl_3): δ (ppm) 8.74 (dt, $J = 4.8, 1.4$ Hz, 1H), 8.44–8.45 (m, 1H), 8.41 (dd, $J = 7.8, 1.5$ Hz, 1H), 7.93

(dd, $J = 7.8, 0.6$ Hz, 1H), 7.81–7.83 (m, 2H), 7.44–7.47 (m, 2H), 7.27–7.35 (m, 4H), 4.88 (s, 2H). $^{13}\text{C-NMR}$ (75 MHz, CDCl_3): δ (ppm) 167.8, 155.1, 150.1, 145.3, 137.1, 136.4, 132.9, 132.5, 132.0, 128.7, 128.6, 127.8, 123.8, 123.5, 121.7, 121.0, 41.7. IR (film): ν (cm^{-1}) 3029, 2930, 1766, 1699, 1617, 1584, 1422, 1387, 1341, 1304, 1155, 1106, 1067, 949, 786, 740, 695, 623. HRMS calcd for $\text{C}_{20}\text{H}_{15}\text{N}_2\text{O}_2$ ($\text{M} + \text{H}$) $^+$ 315.1128, found 315.1124.

***N*-(*tert*-Butyldimethylsilyl)-4-(pyridin-2-yl)phthalimide (2b).** *N*-(*tert*-Butyldimethylsilyl)-4-bromophthalimide (**1b**) (1.10 g, 2.98 mmol) and 2-(trimethylstannyl)pyridine (0.74 g, 3.06 mmol) were dissolved in *m*-xylene (10 mL) and the solution was purged with nitrogen for 20 min. Tetrakis(triphenylphosphine)palladium(0) (40 mg, 35 μmol) was added and the solution heated to reflux under nitrogen for 48 h. The solution was cooled to ambient temperature, water (50 mL) was added, the organic phase was separated, and the aqueous phase was extracted with CH_2Cl_2 twice. The combined organic layers were washed with brine, dried using Na_2SO_4 , filtered, and the solvent removed *in vacuo*. The crude product was subjected to silica gel chromatography with first CH_2Cl_2 and then CH_2Cl_2 -MeOH 50 : 1. The combined product eluents were dried *in vacuo* and *N*-(*tert*-butyldimethylsilyl)-4-(pyridin-2-yl)phthalimide (**2b**) was obtained as a light yellow solid (490 mg, 49%). $^1\text{H-NMR}$ (300 MHz, CDCl_3): δ (ppm) 8.75 (dt, $J = 4.8, 1.3$ Hz, 1H), 8.43 (d, $J = 7.8, 1.5$ Hz, 1H), 8.37–8.38 (m, 1H), 7.90 (dd, $J = 7.8, 0.6$ Hz, 1H), 7.81–7.84 (m, 2H), 7.31–7.35 (m, 1H), 1.00 (s, 9H), 0.55 (s, 6H). $^{13}\text{C-NMR}$ (75 MHz, CDCl_3): δ (ppm) 155.5, 150.3, 145.4, 137.3, 135.0, 134.1, 132.8, 123.6, 123.5, 121.5, 121.2, 26.5, 19.2, –4.1. IR (film): ν (cm^{-1}) 2951, 2926, 2880, 2854, 1759, 1693, 1620, 1585, 1465, 1418, 1350, 1296, 1249, 1155, 1057, 849, 838, 787, 746, 673. HRMS calcd for $\text{C}_{19}\text{H}_{23}\text{N}_2\text{O}_2\text{Si}$ ($\text{M} + \text{H}$) $^+$ 339.1523, found 339.1516.

4-(Tri-*n*-butylstannyl)phthalimide (3). *N*-(*tert*-butyldimethylsilyl)-4-bromophthalimide (**2b**) (100 mg, 294 μmol) was dissolved in toluene (5 mL) and the solution was degassed for 20 min. Hexa-*n*-butylditin (342 μL , 676 μmol) was added followed by the addition of tetrakis(triphenylphosphine)palladium (0) (102 mg, 88 μmol) and the solution was heated to reflux for 5 days. The solvent was removed *in vacuo*, the crude product subjected to silica gel chromatography with first hexane and then hexane-EtOAc 10 : 1. The combined product eluents were dried *in vacuo* and 4-(tri-*n*-butylstannyl)phthalimide (**3**) was obtained as a colourless oil (60 mg, 47%). $^1\text{H-NMR}$ (300 MHz, CDCl_3): δ (ppm) 8.27 (s, 1H), 7.96–7.97 (m, 1H), 7.86 (dd, $J = 7.3, 0.5$ Hz, 1H), 7.77 (dd, $J = 7.2, 0.7$ Hz, 1H), 1.47–1.56 (m, 6H), 1.28–1.36 (m, 6H), 1.10–1.15 (m, 6H), 0.88 (t, $J = 7.3$ Hz, 9H). $^{13}\text{C-NMR}$ (63 MHz, CDCl_3): δ (ppm) 169.3, 168.9, 152.9, 142.2, 132.1, 131.2, 130.9, 122.2, 28.9, 27.3, 13.6, 9.9. IR (film): ν (cm^{-1}) 3253, 2955, 2921, 2853, 1773, 1720, 1459, 1411, 1338, 1294, 1105, 1060, 741, 674. HRMS calcd for $\text{C}_{20}\text{H}_{32}\text{NO}_2\text{Sn}$ ($\text{M} + \text{H}$) $^+$ 438.1453, found 438.1450.

4-(Pyridin-2-yl)phthalimide (2c). 4-(Tri-*n*-butylstannyl)phthalimide (**3**) (30 mg, 69 μmol) and 2-bromopyridine (7.4 μL , 76 μmol) were dissolved in 3 mL *m*-xylene and purged with nitrogen for 15 min. Tetrakis(triphenylphosphine)palladium(0) (8 mg, 6.9 μmol) was added and the mixture heated to reflux for

48 h. The solvent was removed *in vacuo*, the crude product subjected to silica gel chromatography using a gradient of CH_2Cl_2 -MeOH 100 : 1 to 35 : 1. The combined product eluents were dried *in vacuo* and 4-(pyridin-2-yl)phthalimide (**2c**) was obtained as a white solid (10 mg, 65%). $^1\text{H-NMR}$ (300 MHz, DMSO-d_6): δ (ppm) 11.43 (s, 1H), 8.74 (ddd, $J = 4.8, 1.8, 0.9$ Hz, 1H), 8.54 (dd, $J = 7.9, 1.5$ Hz, 1H), 8.47 (dd, $J = 1.5, 0.6$ Hz, 1H), 8.19 (dt, $J = 8.0, 0.9$ Hz, 1H), 7.98 (td, $J = 7.7, 1.8$ Hz, 1H), 7.93 (dd, $J = 7.8, 0.6$ Hz, 1H), 7.47 (ddd, $J = 7.5, 4.8, 1.0$ Hz, 1H). $^{13}\text{C-NMR}$ (63 MHz, DMSO-d_6): δ (ppm) 168.94, 168.91, 153.9, 149.8, 144.3, 137.6, 133.5, 132.6, 132.2, 123.9, 123.4, 121.3, 120.6. IR (film): ν (cm^{-1}) 2926, 2722, 1717, 1655, 1587, 1430, 1351, 1303, 1177, 1141, 1102, 1059, 996, 833, 783, 737, 687, 634. HRMS calcd for $\text{C}_{13}\text{H}_9\text{N}_2\text{O}_2$ ($\text{M} + \text{H}$) $^+$ 225.0659, found 225.0659.

Half-sandwich complex 4. *N*-Benzyl-4-(pyridin-2-yl)phthalimide (**2a**) (20 mg, 64 μmol) was dissolved in methanol (4 mL). Triethylamine (6.4 μL , 77 μmol) was added, followed by $[\text{Ru}(\eta^5\text{-C}_5\text{H}_5)(\text{CO})(\text{MeCN})_2]\text{PF}_6$ (40 mg, 96 μmol), and the solution was stirred for 2 h at 55 $^\circ\text{C}$. The solution was cooled to ambient temperature, CH_2Cl_2 (20 mL) was added, and the solution was washed with brine twice. The organic phase was dried using MgSO_4 , filtered, and evaporated to dryness *in vacuo*. The crude product was subjected to silica gel chromatography with CH_2Cl_2 . The combined product eluents were dried *in vacuo* and the half-sandwich complex **4** was obtained as an orange solid (25 mg, 70%). $^1\text{H-NMR}$ (300 MHz, CDCl_3): δ (ppm) 8.95 (ddd, $J = 5.7, 1.5, 0.7$ Hz, 1H), 7.94 (d, $J = 7.7$ Hz, 1H), 7.91–7.94 (m, 1H), 7.77 (td, $J = 7.8, 1.6$ Hz, 1H), 7.55 (d, $J = 7.5$ Hz, 1H), 7.46–7.48 (m, 2H), 7.27–7.36 (m, 3H), 6.99–7.04 (m, 1H), 5.10 (s, 5H), 4.87 (s, 2H). $^{13}\text{C-NMR}$ (75 MHz, CDCl_3): δ (ppm) 177.8, 170.8, 165.3, 157.6, 153.7, 137.4, 136.7, 132.8, 128.7, 128.6, 127.6, 127.0, 121.7, 120.1, 117.3, 84.8, 41.5. IR (film) ν (cm^{-1}) 3114, 2942, 1906, 1755, 1696, 1590, 1390, 1326, 1267, 1104, 943, 807, 779, 749, 699. HRMS calcd for $\text{C}_{26}\text{H}_{19}\text{N}_2\text{O}_3\text{Ru}$ ($\text{M} + \text{H}$) $^+$ 509.0441, found 509.0427.

Iridium(III) complex 5. *N*-Benzyl-4-(pyridin-2-yl)phthalimide (**2a**) (31 mg, 99 μmol) and PPh_3 (103 mg, 395 μmol) were placed in a flask under nitrogen. $[\text{Ir}(\text{COD})\text{Cl}]_2$ (33 mg, 49 μmol) was added in the glovebox and 2-ethoxyethanol (4 mL) was added. The solution was heated to reflux for 18 h. Upon cooling to ambient temperature, a yellow precipitate was formed that was filtered off and washed three times with methanol. The resulting yellow solid was recrystallized from hexane- CHCl_3 10 : 1 to afford iridium(III) complex **5** as a yellow powder (70 mg, 67%). $^1\text{H-NMR}$ (500 MHz, CDCl_3): δ (ppm) 9.07 (d, $J = 5.4$ Hz, 1H), 7.63 (d, $J = 8.1$ Hz, 1H), 7.59 (s, 1H), 7.48–7.51 (m, 1H), 7.34–7.39 (m, 16H), 7.27–7.30 (m, 1H), 7.07–7.09 (m, 18H), 6.83–6.85 (m, 1H), 6.61 (s, 1H), 4.70 (s, 2H), –16.58 (t, $J = 16.5$ Hz, 1H). $^{13}\text{C-NMR}$ (125 MHz, CDCl_3): δ (ppm) 169.5, 168.0, 165.43, 165.37, 163.6, 150.5, 146.6, 138.3, 137.3, 136.4, 133.93, 133.89, 133.8, 131.6, 131.4, 131.3, 131.2, 129.3, 128.5, 128.3, 127.6, 127.51, 127.47, 127.4, 122.4, 122.2, 118.5, 116.3, 41.0. $^{31}\text{P-NMR}$ (121 MHz, CDCl_3): δ (ppm) 5.4. IR (film): ν (cm^{-1}) 3047, 2926, 2117, 1758, 1696, 1601, 1481, 1431, 1380, 1340, 1184, 1092, 820, 790, 744, 693. HRMS calcd for $\text{C}_{56}\text{H}_{44}\text{ClIrN}_2\text{O}_2\text{P}_2\text{Na}$ ($\text{M} + \text{Na}$) $^+$ 1089.2088, found 1089.2087.

Ruthenium acetonitrile complex 7a. *N*-(Benzyl)-4-(pyridin-2-yl)phthalimide (**2b**) (50 mg, 148 μmol) and $[\text{Ru}(\text{MeCN})_3([\text{9}]\text{-aneS}_3)](\text{CF}_3\text{SO}_3)_2$ (**6**) (156 mg, 222 μmol) were dissolved in DMF (4 mL) and purged with nitrogen for 15 min. Triethylamine (26.8 μL , 192 μmol) was added and the solution heated to 90 $^\circ\text{C}$ for 16 h. The solvent was removed and the crude product subjected to silica gel chromatography with first acetonitrile and then acetonitrile–water–sat. KNO_3 solution 50 : 3 : 1. The combined product eluents were dried *in vacuo*, dissolved in a minimal amount of aqueous acetonitrile, and NH_4PF_6 was added. The solution was centrifuged, the resulting orange filter cake washed three times with water, and dried *in vacuo* to provide the monoacetonitrile complex **7a** as a light orange solid (91 mg, 79%). $^1\text{H-NMR}$ (300 MHz, CD_3CN): δ (ppm) 8.74 (dd, $J = 5.6, 0.8$ Hz, 1H), 8.31 (s, 1H), 8.20 (d, $J = 8.1$ Hz, 1H), 8.17 (s, 1H), 7.90 (td, $J = 7.8, 1.5$ Hz, 1H), 7.26–7.37 (m, 6H), 4.79 (d, $J = 1.6$ Hz, 2H), 2.82–3.08 (m, 4H), 2.59–2.75 (m, 3H), 2.44–2.52 (m, 1H), 2.22–2.40 (m, 3H), 2.08–2.17 (m, 1H), 1.98 (s, 3H). $^{13}\text{C-NMR}$ (63 MHz, CD_3CN): δ (ppm) 196.0, 169.7, 169.1, 164.4, 152.9, 151.4, 137.2, 132.7, 130.7, 126.5, 123.8, 122.8, 120.3, 116.4, 35.0, 33.9, 33.3, 31.3, 30.2, 27.7, 2.8. IR (film): ν (cm^{-1}) 3250, 3028, 1762, 1699, 1599, 1477, 1385, 1353, 1273, 1077, 1014, 834, 748, 696. HRMS calcd for $\text{C}_{28}\text{H}_{28}\text{N}_3\text{O}_2\text{RuS}_3$ ($\text{M} - \text{PF}_6$) $^+$ 636.0387, found 636.0381.

Ruthenium acetonitrile complex 7b. *N*-(*tert*-Butyldimethylsilyl)-4-(pyridin-2-yl)phthalimide (**2b**) (50 mg, 148 μmol) and $[\text{Ru}(\text{MeCN})_3([\text{9}]\text{-aneS}_3)](\text{CF}_3\text{SO}_3)_2$ (**6**) (156 mg, 222 μmol) were dissolved in DMF (5 mL) and purged with nitrogen for 15 min. Triethylamine (26.8 μL , 192 μmol) was added and the solution was heated to 90 $^\circ\text{C}$ for 16 h. The solvent was removed and the crude product subjected to silica gel chromatography with first acetonitrile and then acetonitrile–water–sat. KNO_3 solution 50 : 3 : 1. The combined product eluents were dried *in vacuo*, dissolved in a minimal amount of aqueous acetonitrile, and NH_4PF_6 was added. The solution was centrifuged, the resulting orange filter cake washed three times with water, and dried *in vacuo* to provide the monoacetonitrile complex **7b** as a light orange solid (75 mg, 74%). $^1\text{H-NMR}$ (500 MHz, CD_3CN): δ (ppm) 8.75 (ddd, $J = 5.6, 1.5, 0.7$ Hz, 1H), 8.60 (s, 1H), 8.28 (s, 1H), 8.24 (d, $J = 8.1$ Hz, 1H), 8.17 (s, 1H), 7.92 (ddd, $J = 8.1, 6.7, 1.5$ Hz, 1H), 7.30 (ddd, $J = 7.4, 5.6, 1.4$ Hz, 1H), 2.92–3.06 (m, 3H), 2.83–2.88 (m, 1H), 2.59–2.74 (m, 3H), 2.45–2.50 (m, 1H), 2.33–2.39 (m, 1H), 2.25–2.31 (m, 2H), 2.10–2.16 (m, 1H). $^{13}\text{C-NMR}$ (125 MHz, CD_3CN): δ (ppm) 196.3, 170.0, 169.5, 164.7, 153.2, 151.8, 137.6, 133.0, 131.1, 126.9, 124.1, 120.6, 116.8, 35.4, 34.3, 33.7, 31.6, 30.6, 28.1. IR (film): ν (cm^{-1}) 3185, 3059, 1755, 1704, 1590, 1476, 1444, 1411, 1339, 1307, 1211, 1131, 1044, 835, 747, 677, 645. HRMS calcd for $\text{C}_{21}\text{H}_{22}\text{N}_3\text{O}_2\text{RuS}_3$ ($\text{M} - \text{PF}_6$) $^+$ 545.9916, found 545.9911.

Ruthenium carbonyl complex 8a. Monoacetonitrile complex **7a** (25 mg, 32 μmol) was dissolved in DMF (3 mL), purged with CO gas for 30 s, and heated under a CO atmosphere to 95 $^\circ\text{C}$ for 3 h. The solvent was removed and the crude product subjected to silica gel chromatography with first acetonitrile and then acetonitrile–water–sat. KNO_3 solution 50 : 3 : 1. The combined product eluents were dried *in vacuo*, dissolved in a minimal amount of aqueous acetonitrile, and NH_4PF_6 was

added. The solution was centrifuged, the resulting orange filter cake washed three times with water, and dried *in vacuo* to provide the carbonyl complex **8a** as an orange solid (21 mg, 85%). $^1\text{H-NMR}$ (300 MHz, CD_3CN): δ (ppm) 8.55 (dd, $J = 5.4, 0.6$ Hz, 1H), 8.31–8.34 (m, 2H), 8.12 (s, 1H), 8.06 (dt, $J = 7.5, 1.5$ Hz, 1H), 7.25–7.41 (m, 6H), 4.82 (s, 2H), 3.27–3.36 (m, 1H), 3.10–3.23 (m, 3H), 2.83–2.96 (m, 3H), 2.70–2.81 (m, 2H), 2.53–2.64 (m, 2H), 2.35–2.46 (m, 1H). $^{13}\text{C-NMR}$ (125 MHz, CD_3CN): δ (ppm) 194.2, 180.0, 168.7, 168.6, 163.9, 153.7, 151.0, 139.4, 137.2, 132.8, 131.5, 128.7, 128.4, 127.7, 127.5, 125.2, 121.9, 118.0, 41.1, 37.0, 34.9, 34.8, 33.2, 32.3, 29.8. IR (film): ν (cm^{-1}) 2949, 1978, 1763, 1703, 1600, 1477, 1381, 1271, 1190, 1107, 1032, 966, 829, 750, 722. HRMS calcd for $\text{C}_{27}\text{H}_{25}\text{N}_2\text{O}_3\text{RuS}_3$ ($\text{M} - \text{PF}_6$) $^+$ 623.0071, found 623.0064.

Ruthenium carbonyl complex 8b. Monoacetonitrile complex **7b** (15 mg, 22 μmol) was dissolved in DMF (3 mL), purged with CO gas for 30 s, and heated under a CO atmosphere to 95 $^\circ\text{C}$ for 3 h. The solvent was removed and the crude product subjected to silica gel chromatography with first acetonitrile and then acetonitrile–water–sat. KNO_3 solution 50 : 3 : 1. The combined product eluents were dried *in vacuo*, dissolved in a minimal amount of aqueous acetonitrile, and NH_4PF_6 was added. The solution was centrifuged, the resulting orange filter cake washed three times with water, and dried *in vacuo* to provide the carbonyl complex **8b** as an orange solid (12 mg, 82%). $^1\text{H-NMR}$ (500 MHz, CD_3CN): δ (ppm) 8.81 (s, 1H), 8.55 (ddd, $J = 5.6, 1.5, 0.8$ Hz, 1H), 8.34 (dd, $J = 7.3, 0.7$ Hz, 1H), 8.29 (s, 1H), 8.09 (s, 1H), 8.06 (ddd, $J = 8.1, 7.6, 1.5$ Hz, 1H), 7.39 (ddd, $J = 7.5, 5.6, 1.4$ Hz, 1H), 3.29–3.34 (m, 1H), 3.11–3.21 (m, 3H), 2.91–2.96 (m, 1H), 2.82–2.90 (m, 2H), 2.71–2.79 (m, 2H), 2.57–2.64 (m, 2H), 2.39–2.45 (m, 1H). $^{13}\text{C-NMR}$ (125 MHz, CD_3CN): δ (ppm) 194.3, 179.6, 169.1, 169.0, 163.9, 153.7, 151.1, 139.3, 132.7, 132.3, 129.3, 125.2, 122.0, 117.9, 36.9, 34.9, 34.8, 33.2, 32.3, 29.8. IR (film): ν (cm^{-1}) 3223, 1970, 1765, 1713, 1560, 1480, 1450, 1408, 1343, 1307, 1221, 1171, 1133, 1042, 831, 745, 645. HRMS calcd for $\text{C}_{20}\text{H}_{19}\text{N}_2\text{O}_3\text{RuS}_3$ ($\text{M} - \text{PF}_6$) $^+$ 532.9596, found 532.9606.

Ruthenium isothiocyanate complex 9b. Monoacetonitrile complex **7b** (23 mg, 33 μmol) was dissolved in DMF (3 mL). NaSCN (4 mg, 50 μmol) dissolved in water (300 μL) was added and the solution heated to 90 $^\circ\text{C}$ for 5 h. The solvent was removed and the crude product subjected to silica gel chromatography with CH_2Cl_2 –MeOH 35 : 1 to 10 : 1. The combined product eluents were dried *in vacuo* and the N-bound isomer was obtained as a red solid (8 mg, 47%). Small amounts of the S-bound isomer (2 mg, 9%) were obtained as a purple solid. The coordination mode of the ambidentate thiocyanate ligand was verified by X-ray crystallography of a benzylated derivative.¹⁶

N-bound isomer: $^1\text{H-NMR}$ (300 MHz, DMSO-d_6): δ (ppm) 10.88 (s, 1H), 8.79 (d, $J = 5.1$ Hz, 1H), 8.42 (d, $J = 8.1$ Hz, 1H), 8.20 (s, 1H), 8.18 (s, 1H), 7.91 (t, $J = 7.2$ Hz, 1H), 7.33 (t, $J = 6.3$ Hz, 1H), 2.79–3.02 (m, 4H), 2.42–2.68 (m, 7H), 2.03–2.10 (m, 1H). $^{13}\text{C-NMR}$ (75 MHz, DMSO-d_6): δ (ppm) 201.5, 170.9, 170.2, 164.4, 152.8, 151.3, 136.8, 132.5, 132.1, 130.1, 125.2, 123.7, 120.2, 116.5, 34.7, 34.5, 33.5, 30.9, 30.4, 27.8. IR (film): ν (cm^{-1}) 2961, 2922, 2099, 1752, 1706, 1591, 1558, 1474,

1339, 1305, 1210, 1128, 1035, 820, 790, 722. HRMS calcd for $C_{20}H_{19}N_3O_2RuS_4Na$ ($M + Na$)⁺ 585.9297, found 585.9296.

S-bound isomer: ¹H-NMR (300 MHz, DMSO-*d*₆): δ (ppm) 10.85 (s, 1H), 8.72 (dd, $J = 5.7, 0.9$ Hz, 1H), 8.39 (d, $J = 8.1$ Hz, 1H), 8.17 (s, 1H), 8.08 (s, 1H), 7.84–7.90 (m, 1H), 7.30 (ddd, $J = 7.5, 5.7, 1.2$ Hz, 1H), 2.62–2.93 (m, 11H), 2.07–2.14 (m, 1H). HRMS calcd for $C_{20}H_{19}N_3O_2RuS_4Na$ ($M + Na$)⁺ 585.9297, found 585.9293.

Ruthenium isocyanate complex 10b. Monoacetonitrile complex **7b** (23 mg, 33 μ mol) was dissolved in DMF (3 mL). NaOCN (3 mg, 50 μ mol) dissolved in water (300 μ L) was added and the solution heated to 95 °C for 3 h. The solvent was removed and the crude product subjected to silica gel chromatography with CH_2Cl_2 –MeOH 35:1 to 10:1. The combined product eluents were dried *in vacuo* to provide the isocyanate complex **10b** as a red solid (10 mg, 55%). ¹H-NMR (300 MHz, DMSO-*d*₆): δ (ppm) 10.82 (s, 1H), 8.80 (dd, $J = 5.6, 0.8$ Hz, 1H), 8.37 (d, $J = 8.3$ Hz, 1H), 8.19 (s, 1H), 8.15 (s, 1H), 7.84–7.90 (m, 1H), 7.27–7.31 (m, 1H), 2.73–2.95 (m, 5H), 2.56–2.64 (m, 3H), 2.34–2.45 (m, 3H), 1.99–2.08 (m, 1H). ¹³C-NMR (125 MHz, DMSO-*d*₆): δ (ppm) 205.4, 171.6, 170.8, 164.9, 153.1, 151.8, 136.8, 132.9, 130.3, 125.0, 123.9, 120.4, 116.8, 35.4, 34.8, 34.3, 31.2, 30.7, 28.0. IR (film): ν (cm⁻¹) 3436, 3154, 3052, 2181, 1751, 1700, 1620, 1587, 1473, 1405, 1338, 1306, 1037, 898, 816, 743. HRMS calcd for $C_{20}H_{19}N_3O_3RuS_3Na$ ($M + Na$)⁺ 569.9526, found 569.9520.

Ruthenium selenocyanate complex 11b. Monoacetonitrile complex **7b** (13 mg, 19 μ mol) was dissolved in DMF (3 mL). KSeCN (4 mg, 28 μ mol) dissolved in water (300 μ L) was added and the solution heated to 90 °C for 5 h. The solvent was removed and the crude product subjected to silica gel chromatography with CH_2Cl_2 –MeOH 35:1 to 10:1. The combined product eluents were dried *in vacuo* to provide the selenocyanate complex **11b** as a red solid (11 mg, 96%). The coordination mode of the ambidentate selenocyanate ligand through the

selenium atom was verified by the chemical shift in the ¹³C-NMR spectrum. The signal at 108.2 ppm is in accordance with reported chemical shifts of coordinated selenocyanates.²⁶

¹H-NMR (500 MHz, DMSO-*d*₆): δ (ppm) 10.83 (s, 1H), 8.72 (d, $J = 5.0$ Hz, 1H), 8.38 (d, $J = 8.1$ Hz, 1H), 8.17 (s, 1H), 8.08 (s, 1H), 7.84–7.87 (m, 1H), 7.27–7.30 (m, 1H), 2.86–2.93 (m, 2H), 2.75–2.84 (m, 3H), 2.66–2.74 (m, 1H), 2.44–2.54 (m, 5H), 2.06–2.12 (m, 1H). ¹³C-NMR (125 MHz, DMSO-*d*₆): δ (ppm) 201.8, 171.4, 170.7, 164.6, 153.2, 151.6, 136.7, 132.8, 130.6, 125.6, 124.0, 120.8, 116.9, 108.2, 35.3, 34.7, 33.4, 33.3, 32.4, 28.7. IR (film): ν (cm⁻¹) 3121, 3053, 2920, 2719, 2098, 1749, 1708, 1590, 1473, 1442, 1406, 1336, 1304, 1208, 1139, 1039, 1012, 949, 899, 817, 744. HRMS calcd for $C_{20}H_{19}N_3O_2RuS_3SeNa$ ($M + Na$)⁺ 633.8747, found 633.8734.

Small molecule single crystal X-ray diffraction studies. Single crystals of complexes **4**, **5**, and **8a** were obtained upon slow diffusion of diethyl ether into dichloromethane at 6 °C. Single crystals of complex **7b** were obtained upon slow diffusion of diethyl ether into acetonitrile at 6 °C. The intensity data sets for all compounds were collected at 100 K using a STOE IPDS2 (**4**, **8a**) or IPDS-2T (**5**, **7b**) system. The data were corrected for absorption effects using multi-scanned reflections.²⁷ The structure was solved using direct methods (SIR-92²⁸ for **7b** and **8a**, and SIR2008²⁹ for **4** and **5**) and refined using the full matrix least squares procedure implemented in SHELX-97.³⁰ Hydrogen atoms were included at calculated positions. In complex **5**, the position of the hydrogen atom bonded to iridium has been calculated using XHYDEX (Table 1).³¹

Protein crystallography. The protein was expressed and purified as described previously.^{22a} To a solution of Pim1 (7 mg mL⁻¹) in 50 mM HEPES pH 7.5, 250 mM NaCl, 5 mM DTT, 5% glycerol was added the racemic ruthenium complex **8b** (10 mM DMSO stock solution) to a concentration of 1 mM and the mixture was incubated on ice for 1 h. Crystals of nonphosphorylated Pim1 were grown at 4 °C in 0.6 μ L sitting drops

Table 1 Crystallographic data for **4**, **5**, **7b**, and **8a**^a

	4	5	7b	8a
Formula	$C_{26}H_{18}N_2O_3Ru$	$C_{56}H_{44}ClIr N_2O_2P_2, 1.63 CHCl_3$	$C_{25}H_{32}N_3O_3RuS_3 PF_6$	$C_{27}H_{25}N_2O_3RuS_3 PF_6$
Fw	507.49	1260.49	764.76	767.71
<i>a</i> (Å)	10.9398(5)	9.3488(3)	25.2192(9)	9.1961(5)
<i>b</i> (Å)	11.2895(4)	24.1361(8)	10.9005(5)	12.0944(7)
<i>c</i> (Å)	16.6190(6)	49.146(2)	24.1706(9)	13.5948(8)
α (°)	90	90	90	70.913(4)
β (°)	90	90	115.242(3)	75.580(5)
γ (°)	90	90	90	83.035(5)
<i>V</i> (Å ³)	2052.53(14)	11 089.6(7)	6010.1(4)	1382.58(14)
<i>Z</i>	4	8	8	2
Space group	$P2_12_1$	$Pbca$	$C2/c$	$P\bar{1}$
<i>D</i> _{calcd} (Mg m ⁻³)	1.642	1.510	1.690	1.844
μ (mm ⁻¹)	0.796	2.792	0.854	0.928
θ range (°)	2.18–25.0	2.49–25.0	4.54–25.0	1.63–25.0
No. of indep. reflections	3614	9746	5248	4749
No. of parameters	289	651	442	388
<i>wR</i> ₂ (all data) ^b	0.0462	0.1111	0.1028	0.0865
<i>R</i> ₁ ($I > 2\sigma(I)$) ^b	0.0268	0.0526	0.0383	0.0368
CCDC no.	861334	861335	861336	861337

^a MoK α radiation ($\lambda = 0.71073$ Å). ^b $R_1 = \Sigma||F_o| - |F_c||/\Sigma|F_o|$; $wR_2 = [\Sigma(w(F_o^2 - F_c^2)^2)/\Sigma w(F_o^2)]^{1/2}$.

Table 2 Data collection and refinement statistics for the complex Pim1–8b

Data collection and processing	
X-ray source	ESRF, Grenoble, France
Detector	MarMOSAIC 225
Wavelength (Å)	0.8726
Space group	$P6_5$
Cell dimensions (a, b, c Å/ $\alpha, \beta, \gamma^\circ$)	99.2, 99.2, 80.6 90.0, 90.0, 120.0 24.8–2.3 (2.4–2.3)
Resolution (Å) ^a	128 610 (15 302)
Total reflections ^a	6.4 (6.4)
Multiplicity ^a	20 098 (2386)
Unique reflections ^a	12.8 (51.5)
R_{merge} (%) ^a	99.8 (100.0)
Completeness (%) ^a	16.6 (4.81)
$I/\sigma(I)$ ^a	28.3
Wilson B -factor (Å ²)	
Refinement statistics	
Resolution (Å)	24.8–2.3
$R_{\text{factor}}, R_{\text{free}}$ (%)	17.1, 20.1
Reflections (working, test set)	19 383 (711)
Completeness for range (%)	99.90
rmsd from ideal:	
Bond lengths (Å)	0.014
Bond angles (°)	1.44
Total number of non-hydrogen atoms	2383
Mean B value (Å ²)	24.0

^a In parenthesis is given the value for the highest resolution shell.

using crystallization roboter Cartesian MicrosysTM SQ 4004 (MarXTAL Laboratory, Philipps-University Marburg), where 0.3 μL of protein solution were mixed with 0.3 μL of the precipitate stock containing 200 mM sodium citrate, 100 mM HEPES, 30% MPD pH 7.5 (JCSG Core Suite IV, Qiagen). The final concentration of complex **8b** was 0.5 mM and 5% DMSO resulting from the ruthenium stock solution. Crystals were obtained after 3–5 days and were soaked in the crystallization buffer supplemented with 25% glycerol before being flash frozen in liquid nitrogen. The Pim1–**8b** complex was crystallized in space group $P6_5$ with $\alpha = \beta = 90^\circ$, $\gamma = 120^\circ$ and $a = b = 99.2$ Å and $c = 80.6$ Å. X-ray data were collected at beamline ID23-2 (14.20 keV, 0.8726 Å), European Synchrotron Radiation Facility (ESRF), Grenoble, France at 100 K from a single crystal with a Mar-Mosaic 225 detector system. Data reduction was carried out using XDS and XSCALE.³² The structure was solved with Pim1 coordinates (PDB ID 3BWF)⁶ by molecular replacement using PHASER³³ of the CCP4³⁴ package. The Phaser solution with data up to 2.3 Å yielded one molecule per asymmetric unit with z scores of 24.0 for the rotation function and 55.9 for the translation. Further refinement was carried out with REFMAC5³⁵ and COOT³⁶ at 2.3 Å, which led to 2 outliers (2/273, 0.73%) and 7 residues in allowed regions (4/273, 2.6%) according to the Ramachandran plot. Final statistics reported R -factors of $R_{\text{work}} = 17.1\%$ and $R_{\text{free}} = 20.1\%$ for the Pim1–**8b** complex (Table 2).

Acknowledgements

We thank the National Institutes of Health USA (CA114046) and the German Research Foundation (DFG) for support of this research. We also thank the staff of beamline ID23-2 at the

European Synchrotron Radiation Facility, Grenoble, France for support during data collection. S.B. acknowledges a stipend from the Fonds der Chemischen Industrie.

References

- 1 Metal complexes for medicine and the life sciences: (a) K. H. Thompson and C. Orvig, *Science*, 2003, **300**, 936–939; (b) W. H. Ang and P. J. Dyson, *Eur. J. Inorg. Chem.*, 2006, 4003–4018; (c) T. W. Hambley, *Dalton Trans.*, 2007, 4929–4937; (d) T. W. Hambley, *Science*, 2007, **318**, 1392–1393; (e) A. Mukherjee and P. J. Sadler, *Wiley Encycl. Chem. Biol.*, 2009, 1–47; (f) K. L. Haas and K. J. Franz, *Chem. Rev.*, 2009, **109**, 4921–4960; (g) A. Levina, A. Mitra and P. A. Lay, *Metallomics*, 2009, **1**, 458–470; (h) E. A. Hillard and G. Jaouen, *Organometallics*, 2011, **30**, 20–27; (i) G. Gasser, I. Ott and N. Metzler-Nolte, *J. Med. Chem.*, 2011, **54**, 3–25.
- 2 (a) E. Meggers, *Chem. Commun.*, 2009, 1001–1010; (b) C. L. Davies, E. L. Dux and A.-K. Duhme-Klair, *Dalton Trans.*, 2009, 10141–10154; (c) C.-M. Che and F.-M. Siu, *Curr. Opin. Chem. Biol.*, 2010, **14**, 255–261.
- 3 For recent examples of metal-based enzyme inhibitors, see: (a) D. Can, B. Spingler, P. Schmutz, F. Mendes, P. Raposinho, C. Fernandes, F. Carta, A. Innocenti, I. Santos, C. T. Supuran and R. Alberto, *Angew. Chem., Int. Ed.*, 2012, **51**, 3354–3357; (b) A. J. Salmon, M. L. Williams, A. Hofmann and S.-A. Poulsen, *Chem. Commun.*, 2012, **48**, 2328–2330; (c) J. Spencer, J. Amin, M. Wang, G. Packham, S. S. S. Alwi, G. J. Tizzard, S. J. Coles, R. M. Paranal, J. E. Bradner and T. D. Heightman, *ACS Med. Chem. Lett.*, 2011, **2**, 358–362; (d) F. W. Monnard, T. Heinisch, E. S. Nogueira, T. Schirmer and T. R. Ward, *Chem. Commun.*, 2011, **47**, 8238–8240.
- 4 (a) B. M. Zeglis, V. C. Pierre and J. K. Barton, *Chem. Commun.*, 2007, 4565–4579; (b) F. R. Keene, J. A. Smith and J. G. Collins, *Coord. Chem. Rev.*, 2009, **253**, 2021–2035; (c) M. J. Hannon, *Chem. Soc. Rev.*, 2007, **36**, 280–295; (d) H.-K. Liu and P. J. Sadler, *Acc. Chem. Res.*, 2011, **44**, 349–359.
- 5 (a) L. Feng, Y. Geisselbrecht, S. Blanck, A. Wilbuer, G. E. Atilla-Gokcumen, P. Filippakopoulos, K. Kräling, M. A. Celik, K. Harms, J. Maksimoska, R. Marmorstein, G. Frenking, S. Knapp, L.-O. Essen and E. Meggers, *J. Am. Chem. Soc.*, 2011, **133**, 5976–5986; (b) J. Maksimoska, L. Feng, K. Harms, C. Yi, J. Kissil, R. Marmorstein and E. Meggers, *J. Am. Chem. Soc.*, 2008, **130**, 15764–15765.
- 6 J. Maksimoska, D. S. Williams, G. E. Atilla-Gokcumen, K. S. M. Smalley, P. J. Carroll, R. D. Webster, P. Filippakopoulos, S. Knapp, M. Herlyn and E. Meggers, *Chem.–Eur. J.*, 2008, **14**, 4816–4822.
- 7 S. Dieckmann, R. Riedel, K. Harms and E. Meggers, *Eur. J. Inorg. Chem.*, 2012, 813–821.
- 8 A. Wilbuer, D. H. Vlecken, D. J. Schmitz, K. Kräling, K. Harms, C. P. Bagowski and E. Meggers, *Angew. Chem., Int. Ed.*, 2010, **49**, 3839–3842.
- 9 D. S. Williams, P. J. Carroll and E. Meggers, *Inorg. Chem.*, 2007, **46**, 2944–2946.
- 10 For the design of metal-containing protein kinase inhibitors, see also: (a) J. Spencer, A. P. Mendham, A. K. Kotha, S. C. W. Richardson, E. A. Hillard, G. Jaouen, L. Male and M. B. Hursthouse, *Dalton Trans.*, 2009, 918–921; (b) B. Biersack, M. Zoldakova, K. Effenberger and R. Schobert, *Eur. J. Med. Chem.*, 2010, **45**, 1972–1975.
- 11 For the structure of the catalytic cleft, see: (a) J. Zhang, P. L. Yang and N. S. Gray, *Nat. Rev. Cancer*, 2009, **9**, 28–39; (b) J. J.-L. Liao, *J. Med. Chem.*, 2007, **50**, 409–424.
- 12 (a) H. Bregman, D. S. Williams and E. Meggers, *Synthesis*, 2005, 1521–1527; (b) N. Pagano, J. Maksimoska, H. Bregman, D. S. Williams, R. D. Webster, F. Xue and E. Meggers, *Org. Biomol. Chem.*, 2007, **5**, 1218–1227.
- 13 G. Manning, D. B. Whyte, R. Martinez, T. Hunter and S. Sudarsanam, *Science*, 2002, **298**, 1912–1934.
- 14 S. Blanck, T. Cruchter, A. Vultur, R. Riedel, K. Harms, M. Herlyn and E. Meggers, *Organometallics*, 2011, **30**, 4598–4606.
- 15 For cyclometalated metal complexes with biological activity, see: (a) J.-P. Djukic, J.-B. Sortais, L. Barloy and M. Pfeiffer, *Eur. J. Inorg. Chem.*, 2009, 817–853; (b) X. Meng, M. L. Leyva, M. Jenny, I. Gross, S. Benosman, B. Fricker, S. Harlepp, P. Hébraud, A. Boos, P. Wlosik,

- P. Bischoff, C. Sirlin, M. Pfeffer, J.-P. Loeffler and C. Gaidon, *Cancer Res.*, 2009, **69**, 5458–5466.
- 16 S. Blanck, J. Maksimoska, J. Baumeister, K. Harms, R. Marmorstein and E. Meggers, *Angew. Chem., Int. Ed.*, 2012, **51**, 5244–5246.
- 17 T. P. Gill and K. R. Mann, *Organometallics*, 1982, **1**, 485–488.
- 18 C. Landgrafe and W. S. Sheldrick, *Dalton Trans.*, 1994, 1885–1893.
- 19 See, for example: (a) A. D. Ryabov, V. S. Sukharev, L. Alexandrova, R. Le Lagadec and M. Pfeffer, *Inorg. Chem.*, 2001, **40**, 6529–6532; (b) H. Bregman, P. J. Carroll and E. Meggers, *J. Am. Chem. Soc.*, 2006, **128**, 877–884; (c) S. P. Mulcahy, K. Gründler, C. Frias, L. Wagner, A. Prokop and E. Meggers, *Dalton Trans.*, 2010, **39**, 8177–8182.
- 20 M. A. Fabian, W. H. Biggs III, D. K. Treiber, C. E. Atteridge, M. D. Azimioara, M. G. Benedetti, T. A. Carter, P. Ciceri, P. T. Edeen, M. Floyd, J. M. Ford, M. Galvin, J. L. Gerlach, R. M. Grotzfeld, S. Herrgard, D. E. Insko, M. A. Insko, A. G. Lai, J.-M. Lélías, S. A. Mehta, Z. V. Milanov, A. M. Velasco, L. M. Wodicka, H. K. Patel, P. P. Zarrinkar and D. J. Lockhardt, *Nat. Biotechnol.*, 2005, **23**, 329–336.
- 21 M. W. Karaman, S. Herrgard, D. K. Treiber, P. Gallant, C. E. Atteridge, B. T. Campbell, K. W. Chan, P. Ciceri, M. I. Davis, P. T. Edeen, R. Faraoni, M. Floyd, J. P. Hunt, D. J. Lockhardt, Z. V. Milanov, M. J. Morrison, G. Pallares, H. K. Patel, S. Pritchard, L. M. Wodicka and P. P. Zarrinkar, *Nat. Biotechnol.*, 2008, **26**, 127–132.
- 22 (a) J. É. Debreczeni, A. N. Bullock, G. E. Atilla, D. S. Williams, H. Bregman, S. Knapp and E. Meggers, *Angew. Chem., Int. Ed.*, 2006, **45**, 1580–1585; (b) A. N. Bullock, S. Russo, A. Amos, N. Pagano, H. Bregman, J. É. Debreczeni, W. H. Lee, F. von Delft, E. Meggers and S. Knapp, *PLoS One*, 2009, **4**, e7112; (c) G. E. Atilla-Gokcumen, L. Di Costanzo and E. Meggers, *J. Biol. Inorg. Chem.*, 2011, **16**, 45–50.
- 23 C. Brotschi, G. Mathis and C. J. Leumann, *Chem.–Eur. J.*, 2005, **11**, 1911–1923.
- 24 M. Ranger, D. Rondeau and M. Leclerc, *Macromolecules*, 1997, **30**, 7686–7691.
- 25 D. Yang, Y. Long, H. Wang and Z. Zhang, *Org. Lett.*, 2008, **10**, 4723–4726.
- 26 (a) H. Poleschner, R. Radeglia, M. Kuprat, A. M. Richter and E. Fanghänel, *J. Organomet. Chem.*, 1987, **327**, 7–15; (b) J. M. Bellama and S. K. Tandon, *Inorg. Chim. Acta*, 1985, **102**, 23–27.
- 27 A. L. Spek, *PLATON, A Multipurpose Crystallographic Tool*, Utrecht University, Utrecht, The Netherlands, 1998.
- 28 A. Altomare, G. Cascarano, C. Giacovazzo and A. Guagliardi, *J. Appl. Crystallogr.*, 1993, **26**, 343–350.
- 29 M. C. Burla, R. Caliandro, M. Camalli, B. Carrozzini, G. L. Cascarano, L. De Caro, C. Giacovazzo, G. Polidori, D. Siliqi and R. Spagna, *J. Appl. Crystallogr.*, 2007, **40**, 609–613.
- 30 G. M. Sheldrick, *Acta Crystallogr., A*, 2008, **64**, 112–122.
- 31 A. G. Orpen, *J. Chem. Soc., Dalton Trans.*, 1980, 2509–2516.
- 32 W. Kabsch, *Acta Crystallogr., D: Biol. Crystallogr.*, 2010, **66**, 125–132.
- 33 A. J. McCoy, R. W. Grosse-Kunstleve, P. D. Adams, M. D. Winn, L. C. Storoni and R. J. Read, *J. Appl. Crystallogr.*, 2007, **40**, 658–674.
- 34 Collaborative computational project, number 4, *Acta Crystallogr., D: Biol. Crystallogr.*, 1994, **50**, 760–763.
- 35 G. N. Murshudov, A. A. Vagin and E. J. Dodson, *Acta Crystallogr., D: Biol. Crystallogr.*, 1997, **53**, 240–255.
- 36 P. Emsley, B. Lohkamp, W. G. Scott and K. Cowtan, *Acta Crystallogr., D: Biol. Crystallogr.*, 2010, **66**, 486–501.